

# Phase Crossover induced by Dynamical Many Body Localization in Periodically Driven Long-Range Spin Systems

Mahbub Rahaman,<sup>1</sup> Takashi Mori,<sup>2</sup> and Analabha Roy<sup>1</sup>

<sup>1</sup>Department of Physics, The University of Burdwan, Golapbag, Bardhaman - 713 104, India

<sup>2</sup>RIKEN CEMS, 2-1 Hirosawa, Wako, Saitama, 351-0198, Japan

Dynamical many-body freezing occurs in periodic transverse field-driven integrable quantum spin systems. Under resonance conditions, quantum dynamics causes practically infinite hysteresis in the drive response, maintaining its starting value. We extended this to non-integrable many body systems by reducing the Hamiltonian symmetries through a power-law dependence in spin exchange energy,  $J_{ij} = 1/|i - j|^\beta$ . The dynamics of the integrable short-range Transverse Field Ising Model (TFIM) and non-integrable long-range Lipkin Meshkov-Glick (LMG) models were investigated. In the LMG, the resonance conditions in the driving field suppresses the heating postulated by the *Eigenstate Thermalization Hypothesis* (ETH) by inducing *Dynamical Many Body Localization*, or DMBL. This is in contrast to Many Body Localization (MBL), which requires disorder to suppress ETH. DMBL has been validated by the Inverse Participation Ratio (IPR) of the quasi-stationary Floquet modes. While TFIM has IPR localization for all drive parameters, the LMG exhibits high-frequency localization only at the resonances. IPR localization in the LMG deteriorates with an inverse system size law at lower frequencies, which indicates heating to infinite temperature. Furthermore, adiabatically increasing frequency and amplitude from low values raises the Floquet state IPR in the LMG from nearly zero to unity, indicating a phase crossover. This occurrence enables a future technique to construct an MBL engine in clean systems that can be cycled by adjusting drive parameters only.

Keywords: Dynamical localization, Thermalization, Phase Crossover

Periodically driven Quantum Many Body Systems can experience Dynamical Freezing (DMF) when dynamical hysteresis stops observables from reaching their diagonal averaged values and thermalizing to infinite temperature [1–3]. Under certain resonance conditions in the drive parameters, DMF can cause the response to ‘freeze’ completely to its initial value at all times. This arises as a consequence of additional approximate symmetries that occur at resonance. DMF has been demonstrated via the Rotating Wave Approximation (RWA) in the driven TFIM with nearest neighbour interactions [4] and is shown to be protected when translational invariance is explicitly broken (say, by disorder) [5, 6].

The utilization of Floquet theory simplifies the analysis of time-periodic systems. For closed quantum systems governed by the time-dependent Schrödinger equation, the *Floquet Hamiltonian* allows for a mapping of the time-dependent dynamics into the dynamics of a time-independent effective Hamiltonian, provided the system is strobed at integer multiples of the time period of the drive. The time independent eigenstates of the effective Hamiltonian correspond to quasi-stationary *Floquet Modes* of the original Hamiltonian. The temporal progression of the system comes from phase coefficients that capture the dynamics [7, 8].

Any sufficiently complex non-integrable Many Body System is expected to thermalize according to the Eigenstate Thermalization Hypothesis (ETH) despite

the fact that closed quantum dynamics preserves the memory of the initial state of the system. This arises due to the properties of the matrix elements of observables in typical states[9]. The ETH can be readily adapted to time-periodic systems using Floquet theory (the Floquet-ETH, or FETH). Nonetheless, the conditions for ETH to hold are not particularly strong, and the density matrix of the system can fail to approach one that is described by a thermal expression. In such cases, the system is said to undergo *Many Body Localization* (MBL)[10]. This phenomenon is stable against local perturbations, and constitutes an exotic state of matter with far-reaching implications in theoretical physics, as well as in practical applications[11].

The addition of disorder has been identified as a crucial component in the onset of MBL. In that case, thermalization is prevented by disorder-induced localization. An alternative approach to realizing MBL in clean many-body system involves *Floquet Engineering*, where a time-periodic drive is introduced, and the drive parameters tuned so as to introduce a clustering of quasistationary energies in a manner similar to localization[9].

In this article, we propose that additional approximate symmetries can be Floquet-engineered in quantum many body systems with lower symmetry than the TFIM, such as those with long-range interactions. This results in both DMF and MBL occurring simultaneously at resonant values of the drive parameters, and complete thermal behaviour at other values. This

phenomenon is distinct from DMF in the TFIM, since  
clean TFIM systems, being integrable, never thermalize.

To demonstrate the onset of MBL, we investigate the driven Lipkin-Meshkov-Glick (LMG) model, a long-range system that is a special case of the more general Curie-Weiss model, wherein the nearest-neighbour exchange in the TFIM is extended to longer ranges with a power law dependence,  $J_{ij} \sim 1/|i - j|^\beta$  [12-14]. Setting  $\beta = \infty$  recovers the TFIM, and setting  $\beta = 0$  yields the LMG model. We have recovered the onset of DMF in this system and have supported our result with numerical simulations.

In addition, we compare the degree of localization of the quasi-stationary Floquet modes in both limits of  $\beta$ . In order to do so, we look at the Inverse Participation Ratio (IPR) of the Floquet modes in the representation given by the eigenstates of the symmetry-breaking field. The IPR, closely related to the concept of quantum purity, is defined as the formal sum of the square of the density in some physically meaningful space or representation. A high IPR of a stationary state denotes low participation in most of the representation, and a low IPR distributes participation uniformly across the representation, leading to ergodic dynamics[15]. Thus, IPR [16] is a useful tool for witnessing MBL of a quantum system. For an MBL system, the IPR is unity, and it scales inversely with the system size when it is thermally distributed [17].

In the first section of this paper, we present all essential theoretical frameworks. Our results for the LMG model are presented next in section II. In that section, we have used the Rotating Wave Approximation (RWA) [18], where only the slowest rotating terms in the Fourier expansion of the Hamiltonian in a frame co-rotating with the symmetry breaking drive field are retained. In addition, we have the obtained analytical expressions for the Floquet modes and their IPR. They are used to probe the system dynamics in the high and low-frequency domains at both limits of  $\beta$ . In section III we have used phase space plots to contrast the low and high frequency limits of the LMG model in the thermodynamic limit by mapping it to an equivalent classical Hamiltonian system. Finally, in section IV, we have looked at numerical computations of the IPR of the Floquet modes for different values of the drive parameters, well beyond those that allow for the RWA. We observed that, if the system is driven by an adiabatically increasing drive frequency from low to high limit while remaining in the resonance region, a sharp crossover from a thermal to an MBL phase occurs. We conclude with discussions and outlook.

## I. BACKGROUND

The Eigenstate Thermalization Hypothesis (ETH) is a series of conjectures that allows for the thermalization of an isolated quantum many body system. The state of the system,  $|\psi(t)\rangle$ , evolves according to the Schrödinger equation  $\hat{H}|\psi(t)\rangle = i\frac{\partial}{\partial t}|\psi\rangle$ . The Hamiltonian  $\hat{H}$  is assumed to be *non-integrable*, in that it lacks an extensive number of *local* additive conserved quantities, that is to say, there are no set of observables  $\hat{O}_s$  such that  $\hat{H} = \sum_s \hat{O}_s$  for any extensive index  $s$ . Here, the  $\hat{O}_s$  constitute an arbitrary CSCO (complete set of commuting observables) that are *local*, having sub-extensive support in the system size. In addition, we postulate the existence of an equivalent Hamiltonian  $\hat{H}_{eq}$  for every Hamiltonian  $\hat{H}$  as well as an "equilibrium" value  $A_{eq}$  for every observable  $\hat{A}$ , such that

$$A_{eq}(E) \equiv \frac{\text{Tr}(\hat{A}e^{-\beta\hat{H}_{eq}})}{\text{Tr}(e^{-\beta\hat{H}_{eq}})}. \quad (1)$$

where  $E = \langle\psi(t)|\hat{H}|\psi(t)\rangle$  is the conserved energy of the system, and  $\beta = 1/(k_B T)$  is the inverse temperature,  $H_{eq}$  is an effective Hamiltonian that captures the long-time average dynamics of the system, and  $k_B$  is the Boltzmann constant.

To put it simply, ETH proposes that this many-body Hamiltonian undergoes thermalization as seen in the *long-time averages* of observables, with the eigenstates bearing resemblance to thermal states. The aforementioned hypothesis serves as a valuable instrument for comprehending the conduct of simulated quantum systems and their correlation with thermal equilibrium. This assertion can be justified by examining the expectation value of an observable  $\hat{A}$  as it evolves under the Schrödinger equation. To see this, we first expand the state of the system  $|\psi(t)\rangle$  as:

$$|\psi(t)\rangle = \sum_m c_m(t) |m(0)\rangle,$$

where  $|m(0)\rangle$  represents the eigenstates of  $\hat{H}(0)$  with energy  $E_m$ . The coefficients  $c_m(t)$  describe the time-dependent amplitude of the expansion. Plugging these expansions into the expression for the expectation value, we obtain the long-time average of the expectation value [19]:

$$\overline{\langle \hat{A}(t) \rangle} = \sum_{m,k} \overline{c_m^*(t)c_k(t)} \langle m(0)|\hat{A}|k(0)\rangle, \quad (2)$$

where the overline indicates the following operation for any time-dependent quantity  $\mathcal{O}(t)$ ,

$$\overline{\mathcal{O}} \equiv \lim_{T \rightarrow \infty} \frac{1}{T} \int_0^T dt \mathcal{O}(t). \quad (3)$$

Had the system been integrable, the large number of conserved quantities would restrict mixing between the states during unitary evolution. In the non-integrable case, the system explores the entire Hilbert space spanned by eigenstates with eigenvalues close to  $E$  more-or-less uniformly. In that case, the matrix elements  $\langle m(0)|\hat{A}|k(0)\rangle$  are said to satisfy the Srednicki ansatz [20, 21]:

$$\langle m(0)|\hat{A}|k(0)\rangle \approx A_{eq} \left( \frac{E_m + E_k}{2} \right) \delta_{mk} + e^{-\frac{1}{2}S\left(\frac{E_m+E_k}{2}\right)} f\left(\frac{E_m + E_k}{2}, E_m - E_k\right) R_{mk}. \quad (4)$$

Here,  $S$  is the thermodynamic entropy and  $R_{mk}$  are elements of a random matrix with vanishing mean and unit variance. What this means for the ensuing dynamics is that the system explores the accessible Hilbert space uniformly, and the matrix elements  $\langle m(0)|\hat{A}(t)|k(0)\rangle$  become indistinguishable for most pairs of  $m$  and  $k$ . Applying this ansatz and taking the thermodynamic limit by ignoring terms  $\mathcal{O}(e^{-S/2})$ , the expression for the expectation value becomes:

$$\overline{\langle \hat{A}(t) \rangle} \approx \sum_m \overline{|c_m(t)|^2} A_{eq} \left( \frac{E_m + E_k}{2} \right) \approx A_{eq}(E) \sum_m \overline{|c_m(t)|^2} = A_{eq}(E),$$

where, in the last step, we utilized the fact that  $A_{eq}$  is a smooth function, and that the states with energies far from  $E$  have  $|c_m(t)|^2 \approx 0$ . Therefore, in the limit of large systems the expectation value of an observable  $\hat{A}$  is approximately equal to the thermal expectation value  $A_{eq}$ . This is the essence of the ETH, which suggests that individual eigenstates of a quantum system can be described by statistical mechanics in the long-time limit.

We now generalize the ETH to non-integrable many-body systems that are closed, but not isolated. In that case, it is possible to impart a periodic time-dependence on the Hamiltonian while still ensuring unitary evolution. If the time period of the drive is  $T$ , and the corresponding drive frequency  $\omega \equiv 2\pi/T$ , the Floquet theorem states that the solutions to the Schrödinger equation can be written as  $|\psi(t)\rangle = e^{-i\epsilon t/\hbar} |\phi(t)\rangle$ , where the  $|\phi(t)\rangle$  are  $T$ -periodic states called *Floquet Modes*, the corresponding  $\epsilon \in \mathbb{R}$ , are called *quasienergies*. Quasienergy values are not unique, and can be made to be bounded within a Floquet photon, viz. a range  $[-\omega/2, \omega/2]$  [22, 23]. As a consequence, the unitary evolution operator can be split into two parts as follows [24].

$$U(t) = e^{-i\hat{K}_F(t)} e^{-i\hat{H}_F t}. \quad (5)$$

Here, the micromotion operator  $\hat{K}_F(t)$  is time-periodic in  $T$ , with  $\hat{K}_F(0) = 0$ , and the Floquet Hamiltonian  $\hat{H}_F = \hat{H}(t) - i\frac{\partial}{\partial t}\Big|_{t=T}$ . Thus, if the system is strobed at integer multiples of  $T$  only, then the unitary evolution matches that of a time independent Hamiltonian  $H_F$ . This can capture most of the exact dynamics at large frequencies.

In such systems, the Floquet Eigenstate Thermalization Hypothesis (FETH) posits that, subject to specific conditions and in the context of a system of significant size, the Floquet modes themselves exhibit thermal state-like behavior, i.e.,  $\hat{H}_{eq} \approx \hat{H}_F$  in eqn 1. However, in contrast to the isolated systems, the loss of energy conservation allows for the mixing of all Floquet modes in the ensuing dynamics, not just those with quasienergies near  $E$ . Were this to actually happen in the ensuing dynamics, it can be reconciled with ETH [25] by ensuring that  $\beta = 0$  in eq 1. In other words, the nonequilibrium steady state of the system tends to an infinite temperature, maximum entropy density matrix.

However, drive parameters like amplitude, frequency, and duty-cycle strongly affect the structure of the Floquet modes  $|\phi\rangle$ . Thus, they can be engineered to prevent the kind of full mixing that would lead to infinite temperatures, manifesting suppression of thermalization dynamically. Thus, this type of *Floquet Engineering* can produce *Dynamical Many Body Localization* (DMLB), where the system fails to reach thermal equilibrium and remains localised, possibly near its initial state, even at large times. This paradigm seems similar to standard Many-Body Localization [26, 27], where disorder, locality, and integrability can cause athermalism via breakdown in the Srednicki ansatz. However, DMLB is a purely dynamical phenomenon, and thus can occur regardless of disorder, locality of observables, or system integrability, all of which have been studied for MBL onset [28–30].

Integrable Many Body systems do not exhibit thermalization. When subjected to time-periodic drives, Floquet engineering allows for the introduction of additional approximate conserved quantities that dynamically suppress the evolution of certain observables by hysteresis. This type of *freezing* of response has been shown in integrable systems [6]. A paradigmatic example is the driven Transverse Field Ising model (TFIM) in one dimension [31]. The Hamiltonian

is given by

$$\hat{H}(t) = \hat{H}_0 + h_z(t) \hat{H}_1 \quad (6)$$

$$\hat{H}_0 = -\frac{1}{2} \sum_{i=1}^N \sigma_i^x \sigma_{i+1}^x \quad (7)$$

$$\hat{H}_1 = -\frac{1}{2} \sum_{i=1}^N \sigma_i^z. \quad (8)$$

Here, the undriven Hamiltonian  $\hat{H}_0$  consists of nearest-neighbour interactions between  $N$  number of spin-1/2 particles on a one-dimensional spin network. The transverse field is denoted by  $\hat{H}_1$ , and is being varied by a time-periodic and harmonic signal  $h_z(t) = h_0 + h \cos \omega t$ , yielding a time period  $T = 2\pi/\omega$  with amplitude  $h$ , drive frequency  $\omega$ , and d.c. field  $h_0$ . This Hamiltonian can be readily transformed into a spinless pseudo-fermionic system via the Jordan-Wigner transformation [4]. When written in momentum space spanned by spinors  $\psi_k = (c_{-k}, c_k^\dagger)^T$  of fermions at momentum  $k$  created (annihilated) by operators  $c_k^\dagger$  ( $c_k$ ), the effective Hamiltonian

$$H(t) = \sum_{(k,-k)-\text{pairs}} \psi_k^\dagger \left[ \left( f_k - h_z(t) \right) \tau_z + \tau_x \Delta_k \right] \psi_k \quad (9)$$

with  $f_k = J \cos k$ ,  $\Delta_k = J \sin k$ ,  $\tau_{xyz}$  are the three Pauli Matrices, and the sum is over distinct  $(k, -k)$  Cooper Pairs. We can transform our system to a frame that rotates with the time-varying symmetry-breaking field. This is achieved by the means of the unitary transformation operator

$$U(t) = \prod_k U_k(t) \quad (10)$$

$$U_k(t) = \exp \left\{ \left[ \frac{i\hbar}{\omega} \sin \omega t \right] \tau_z \right\}.$$

The resulting transformed Hamiltonian  $H'(t) = U^\dagger(t) H(t) U(t) - iU^\dagger(t) \partial_t U(t)$  simplifies to

$$H'(t) = \sum_{(k,-k)-\text{pairs}} \psi_k^\dagger \left[ \tau_z f_k + \tau_x \cos(\eta \sin \omega t) + \tau_y \sin(\eta \sin \omega t) \right] \psi_k, \quad (11)$$

where we defined  $\eta = 2h/\omega$ . Using the Jacobi-Anger formula [32]

$$e^{i\eta \sin \omega t} = \sum_{n=-\infty}^{\infty} J_n(\eta) e^{in\omega t}, \quad (12)$$

where  $J_n(\eta)$  are Bessel Functions, the transformed Hamiltonian simplifies to

$$H'(t) = \sum_{(k,-k)-\text{pairs}} \psi_k^\dagger \left\{ \tau_z f_k + 2\tau_x \Delta_k \sum_{n \geq 0} J_{2n}(\eta) \cos(2n\omega t) - 2\tau_y \Delta_k \sum_{n \geq 0} J_{2n+1}(\eta) \sin[(2n+1)\omega t] \right\} \psi_k, \quad (13)$$

In the frequency regime  $\omega \gg f_k$ , the long-time average  $H^{RWA} \equiv \lim_{n \rightarrow \infty} \frac{1}{nT} \int_0^{nT} dt H'(t)$  can serve as a suitable approximation for  $H'(t)$ . This approximation, known as the *Rotated Wave Approximation* (RWA), eliminates the oscillating modes and results in an effective Hamiltonian that is independent of time.

$$H^{RWA} = \sum_{(k,-k)-\text{pairs}} \psi_k^\dagger \left[ f_k \tau_z + 2J_0(\eta) \Delta_k \tau_x \right] \psi_k, \quad (14)$$

It is evident that by manipulating the drive parameters, specifically the amplitude denoted by  $h$  and the frequency denoted by  $\omega$ , in a manner such that  $\eta$  is positioned on a root of  $J_0(\eta)$ , the fermion number can be conserved to a significant extent at this particular resonance. Consequently, it is feasible to exercise direct control over  $H^{RWA}$ , resulting in a comprehensive suppression of the dynamics of otherwise responsive observables.

This phenomenon is highly general in nature, and can be readily adapted to non-integrable systems. In such cases, freezing has the additional effect of inducing DMBL, suppressing thermalization to infinite temperatures. Numerical quantification of localization of a specific (quasi) stationary state in a physically significant representation can be achieved through the computation of the *Inverse Participation Ratio* (IPR). In the position representation, the IPR for a state  $|\psi\rangle$  [33-36] is defined as

$$\phi_{IPR} \equiv \int dx |\langle x | \psi \rangle|^4$$

This definition can be generalized to the IPR of a state  $|\phi\rangle$  in a representation given by complete orthonormal basis  $|m\rangle$  as

$$\phi_{IPR} \equiv \sum_m |\langle m | \psi \rangle|^4. \quad (15)$$

The smallest value of the IPR corresponds to a fully delocalized state,  $\psi(x) = 1/\sqrt{N}$  for a system of size  $N$  [36, 37]. Values of the IPR close to unity correspond to localized states [38]. For a periodically driven system, we look at the IPR of the quasi-stationary Floquet modes at  $t = T$ , where  $t = 2\pi/\omega$  for drive frequency  $\omega$ .

In the TFIM model, equation 14 indicates that, at resonance, when  $J_0(\eta) = 0$ , the Floquet modes are approximately given by the fermionic Fock states, which have a trivially unit IPR in the representation of the eigenmodes of the transverse field  $\hat{H}_1$  in equation 6. Here, a particular Floquet mode can be decomposed into a direct product of cooper-pair states as  $|\phi\rangle = \prod_{k,-k} |\phi_k^n\rangle$ . In the RWA limit and at resonance,  $|\phi_k^n\rangle$  has values of  $|0\rangle, |k, -k\rangle$  for two values of  $n = 0, 1$  respectively. We define the reduced IPR of  $|\phi_k^n\rangle \forall k$  to be

$$\phi_{IPR}^{(n)}(k) = |\langle 0 | \phi_k^n \rangle|^4 + |\langle +k, -k | \phi_k^n \rangle|^4, \quad (16)$$

where  $n = 0, 1$ . In the RWA limit and at resonance, this quantity is unity, indicating very low participation and the onset of freezing. Figure 1 shows results

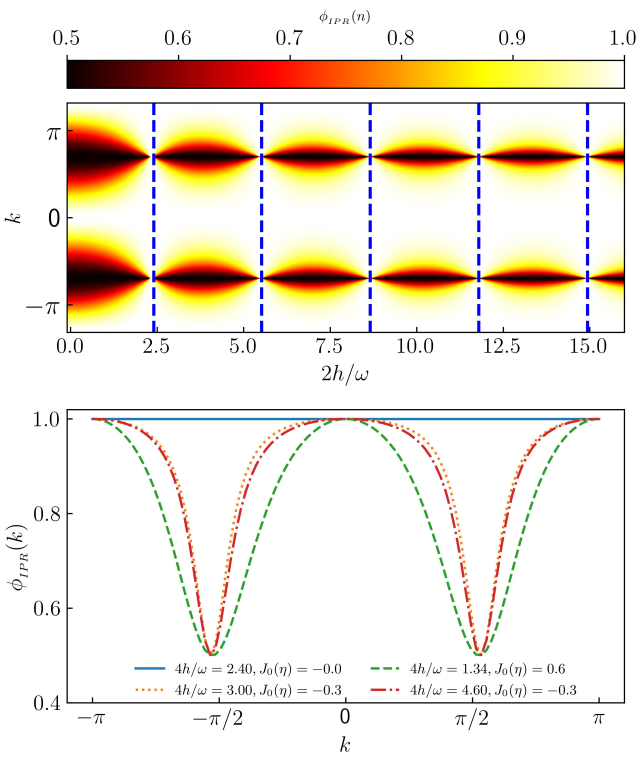


FIG. 1. Reduced IPR (defined in equation 16) for one of the two Floquet modes obtained from the exact dynamics of the TFIM for size  $N = 100$  and  $\omega = 90$  for the entire Brillouin zone (top panel, ordinate) and a few drive amplitudes (top panel, abscissa). The dashed lines (top panel) indicate the roots of  $J_0(\eta)$ . The bottom panel shows cross-sections for four different chosen amplitudes.

from numerically simulating the TFIM dynamics. The reduced IPR for a particular Floquet mode recovered by simulating the exact Schrödinger dynamics over a single time period of the drive, and plotted as a function of momentum  $k$  for different  $\eta$ 's. At resonance, when  $\eta$  lies at the root of the Bessel function  $J_0(\eta)$ ,

the IPR is exactly unity for all momenta. Outside this resonance, the IPR is unity only for some momenta because the effective Hamiltonian is perfect diagonal at  $k \in \{-\pi, 0, \pi\}$  as can be seen in the cross-sectional plots of figure 1. As we move away from the resonance point, IPR reduces from unity. However, as the TFIM is an integrable spin model, the IPR never drops to a value that is small enough to indicate thermalization. At low frequencies, RWA fails due to the unavailability of zero off-diagonal terms in the effective transformed Hamiltonian, as well as the absence of integrability breaking terms to counteract the off diagonal terms. Consequently, the IPR remains quite high ( $\sim 0.5$ ) even at the resonance point as can be seen figure ???. At low frequency, this is valid for all momentum and parameter  $\eta$ , see figure 2.

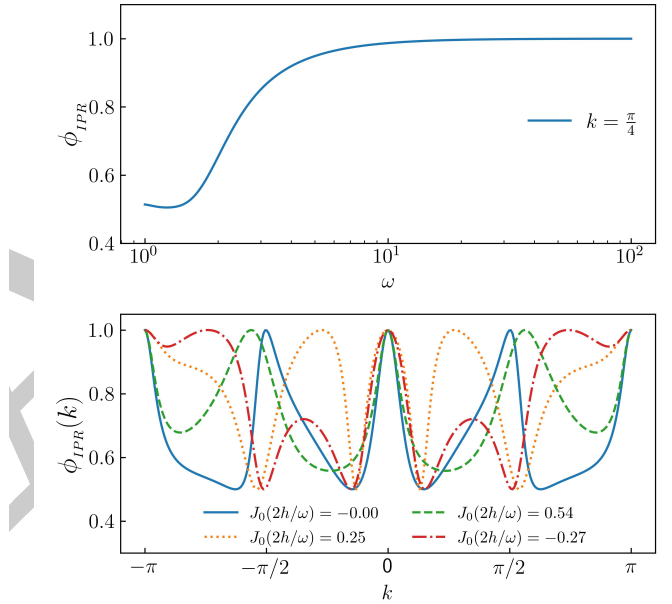


FIG. 2. Reduced IPR obtained by adiabatically increasing  $\omega$  (top panel abscissa) for one the floquet mode obtained from equation 16 at the root of  $J_0(\eta)$  for  $N = 500$ . IPR is  $\sim 0.5$  (localized yet not fully freezing) upto  $\omega \sim 2$ , afterthat, smoothly increased to unity (fully localized and freezibg) at higher  $\omega \geq 10$  (top panel, ordinate). At bottom panel cross-sections for four chosen amplitudes at  $\omega = 2$  are plotted for a brillouin zone (abscissa) with corresponding reduced IPRs(ordinate).

Because the dependence of observable expectations on the eigenstates is always fairly strong for integrable systems like the TFIM, such systems will never exhibit any kind of thermal behaviour unless integrability breaking terms (such as strong disorder) are included [6]. As a result, it is not physically meaningful to refer to the unit IPR region as "Many Body Localization", because the parameter space lacks a thermal-

ized region to contrast with this state. The type of Floquet Engineering described above, on the other hand, can be easily applied to a broad class of nonintegrable systems where FETH is expected to hold in certain regions. Long-range spin systems, in particular, where the exchange energies between far-off spins are taken into account in the model Hamiltonian, are good candidates because they are known to thermalize when driven with low frequencies [39].

## II. LONG RANGE INTERACTIONS: THE LIPKIN MESHKOV GLICK MODEL:

The periodically driven Curie-Weiss model for  $N$  long-range spins is described by the Hamiltonian

$$\hat{H}(t) = \hat{H}_0 + [h \cos(\omega t) + h_0] \hat{H}_1. \quad (17)$$

Here, the undriven part  $\hat{H}_0$  and the driven part  $\hat{H}_1$  are, respectively,

$$\begin{aligned} \hat{H}_0 &= \frac{1}{2} \sum_{ij} J_{ij} \hat{\sigma}_i^z \hat{\sigma}_j^z, \\ \hat{H}_1 &= \sum_{i=1}^N \hat{\sigma}_i^x. \end{aligned} \quad (18)$$

The Heisenberg exchange energy of the bond between spins  $i$  and  $j$  is given by

$$J_{ij} = \frac{J_\alpha}{N^{1-\alpha}} \frac{1}{r_{ij}^\alpha}, \quad (19)$$

with  $r_{ij}$  representing the smallest graph distance between them. Putting  $\alpha = 0$  yields the Lipkin Meshkov Glick (LMG) model with all-to-all interactions  $J_{ij} = J_0/N \forall (i, j), i \neq j$ . We choose to maintain the extensivity of the interaction energy by enforcing the condition

$$\frac{J_0}{N} \sum_{i \neq j} 1 = \frac{J_0}{N} \frac{N(N-1)}{2} = 1,$$

yielding the Kac-norm  $J_0 = 2/(N-1)$ . The Hamiltonian in equation 17 commutes with  $P_{ij} \equiv \frac{1}{2}(1 + \vec{\sigma}_i \cdot \vec{\sigma}_j)$ . In addition, it also commutes with the total angular momentum  $S^2 = |\vec{S}|^2$ , where  $\vec{S} =$

$S^x \hat{x} + S^y \hat{y} + S^z \hat{z} \equiv \frac{1}{2} \sum_i \vec{\sigma}_i$ . We now choose to populate the system in a state with  $S^2 = \frac{N}{2} \left( \frac{N}{2} + 1 \right)$ . In that case, the dynamics remains invariant in the  $N+1$ -dimensional space spanned by the common eigen states of  $P_{ij}, |S|^2$  and  $S_z$ ; the so-called *Totally Symmetric Subspace*, or TSS [40]. Let the eigenvalues of  $S^z$  in the TSS be  $s_n$ , and the eigen vectors be  $|s_n\rangle$ . Here,  $s_n = -\frac{1}{2} + \frac{n}{N}$  and the index  $n = 0(1)N$  has  $N+1$  values. The dynamics is restricted to this invariant subspace, wherein the matrix elements of the Hamiltonian are given by

$$\begin{aligned} \langle s_i | \hat{H}_0 | s_j \rangle &= -\frac{4}{N-1} s_i^2 \delta_{ij}, \\ \langle s_i | \hat{H}_1 | s_j \rangle &= \left[ \sqrt{\frac{N}{2} \left( \frac{N}{2} + 1 \right) - N s_i (N s_{i+1}) \delta_{i+1,j}} \right. \\ &\quad \left. + \sqrt{\frac{N}{2} \left( \frac{N}{2} + 1 \right) - N s_i (N s_{i-1}) \delta_{i-1,j}} \right] \end{aligned} \quad (20)$$

These allow for a numerical representation of the Hamiltonian in the TSS.

Next, we transform the Hamiltonian to the rotated frame given by the operator

$$\hat{U}(t) = \exp \left[ i \frac{h}{\omega} \sin(\omega t) \hat{H}_1 \right]. \quad (21)$$

This is analogous to the rotation performed for the TFIM in eqns 10 and 11. Defining  $\tau = \frac{h}{\omega} \sin \omega t$ , we use the fact that  $\hat{H}_1 = 2S^x$ , as well as the following identity obtained by using the Baker-Campbell-Hausdorff formula,

$$e^{i2\tau \hat{S}^x} \hat{S}^z e^{-i2\tau \hat{S}^x} = \hat{S}^z \cos(2\tau) + \hat{S}^y \sin(2\tau), \quad (22)$$

to simplify the transformed Hamiltonian  $\tilde{H}(t) = \hat{U}^\dagger(t) \hat{H}(t) \hat{U}(t) - \hat{U}^\dagger(t) \partial_t \hat{U}(t)$ , yielding

$$\begin{aligned} \tilde{H}(t) &= -\frac{1}{N-1} \left[ (S^z)^2 (1 + \cos 4\tau) + (S^y)^2 (1 - \cos 4\tau) \right. \\ &\quad \left. + \{S^y, S^z\} \sin 4\tau \right] - 2h_0 S^x. \end{aligned} \quad (23)$$

Next, we define  $\eta \equiv 4h/\omega$  and use the Jacobi-Anger formula in eqn 12 to expand  $\tilde{H}(t)$ . Ignoring constant terms, this yields

$$\tilde{H}(t) \sim \frac{(\hat{S}^x)^2}{N-1} - 2h_0\hat{S}^x - \frac{J_0(\eta)}{N-1} \left[ (\hat{S}^z)^2 - (\hat{S}^y)^2 \right] - \frac{2}{N-1} \sum_{k=1}^{\infty} J_{2k}(\eta) \left[ (\hat{S}^z)^2 - (\hat{S}^y)^2 \right] \cos(2k\omega t) - \frac{2}{N-1} \sum_{k=1}^{\infty} J_{2k-1}(\eta) \{ \hat{S}^y, \hat{S}^z \} \sin[(2k-1)\omega t]. \quad (24)$$

If  $\omega$  is large enough to smooth out the harmonic components, we obtain the RWA,

$$\tilde{H}(t) \approx \tilde{H}_{\text{RWA}} \equiv \frac{(\hat{S}^x)^2}{N-1} - 2h_0\hat{S}^x - \frac{J_0(\eta)}{N-1} \left[ (\hat{S}^z)^2 - (\hat{S}^y)^2 \right]. \quad (25)$$

If the drive amplitude  $h$  is adjusted such that  $\eta$  lies at a root of  $J_0(\eta)$  (the localization point), the RWA Hamiltonian is diagonal in the representation of the transverse field  $\hat{S}^x$ , yielding an IPR of unity in that representation, similar to the TFIM in the previous section. Note however, that if the DC transverse field  $h_0$  is set to 0, then, at the localization point, the RWA Hamiltonian  $\tilde{H}_{\text{RWA}} \sim (\hat{S}^x)^2$ . The eigenvalues are two-fold degenerate. This produces infinitely many (Floquet) eigenmodes in the degenerate subspace whose IPRs may not always be unity in the  $S^x$  representation. The removal of this degeneracy necessitates the inclusion of the d.c. field  $h_0$ . However, note that rational values of  $h_0$  may add accidental degeneracies in  $\tilde{H}_{\text{RWA}}$ . To see this, note that, at a localization point, the eigenvalues of  $\tilde{H}_{\text{RWA}}$  in the TSS are given by

$$\text{Eigs}[\tilde{H}_{\text{RWA}}] = \frac{\left(\frac{N}{2} - m\right)^2}{N-1} - 2h_0 \left(\frac{N}{2} - m\right), \quad (26)$$

where the half-integer  $-N/2 \leq m \leq N/2$  is the eigenvalue corresponding to a particular eigenstate  $|m\rangle$  of the symmetry-breaking field  $\hat{S}^x$ . In order to ensure that no additional degeneracies occur, we have to set  $h_0$  in such a way that no two energies accidentally coincide. If  $N \gg 1$  (substantially large), then this condition can be readily met by assuring that  $(1 - 2h_0)^{-1}$  is never an integer that is divisible by  $N$ . To ensure this in our numerical simulations, we have kept  $h_0$  at a small irrational value.

The localization of the Floquet states at resonance is supported by exact numerical results, as can be seen in fig 3. Here, we show plots of the IPR of the Floquet modes  $|\phi^n\rangle$  for  $S^2 = (N/2)(N/2 + 1)$ . The IPR in  $S^x$  representation is

$$\phi_{\text{IPR}}(n) = \sum_m |\langle m | \phi^n \rangle|^4. \quad (27)$$

These plots were obtained numerically by diagonalizing the propagator  $U(t)$  at  $t = T$ , where  $U(t)$  is defined

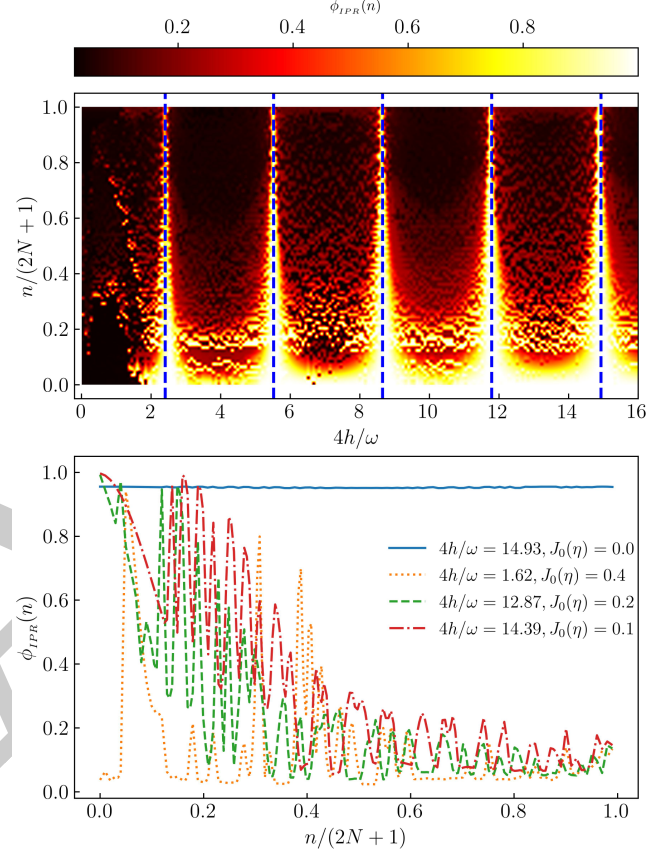


FIG. 3. IPR density plot for all possible Floquet modes (top panel ordinate) for different values of  $\eta = 4h/\omega$  (top panel abscissa), deduced from equation 27 for exact LMG Hamiltonian for  $N = 50$ . Blue dashed lines are roots of  $J_0(\eta)$ . At bottom panel cross-section of IPR (ordinate) for four different  $\eta$ 's plotted for all possible floquet modes (bottom panel, abscissa) at  $\omega = 90$ . IPR founds to be  $\sim$  unity for all floquet modes at roots of  $J_0$ .

in eqn 5. This propagator was obtained from simulations of the exact quantum dynamics using QuTiP, the Quantum Toolbox in Python [41]. We kept the frequency at a fairly large value  $\omega = 90$  where we expect that RWA would be valid, and  $N = \mathcal{O}(10^2)$ . The density plot in the upper panel of fig 3 depicts the IPR of the Floquet states; the abscissa  $\eta = 4h/\omega$  and the ordinate is  $n/(2N+1)$ , where  $n \leq 2N$  is a nonnegative integer that indexes the Floquet states in increasing order of

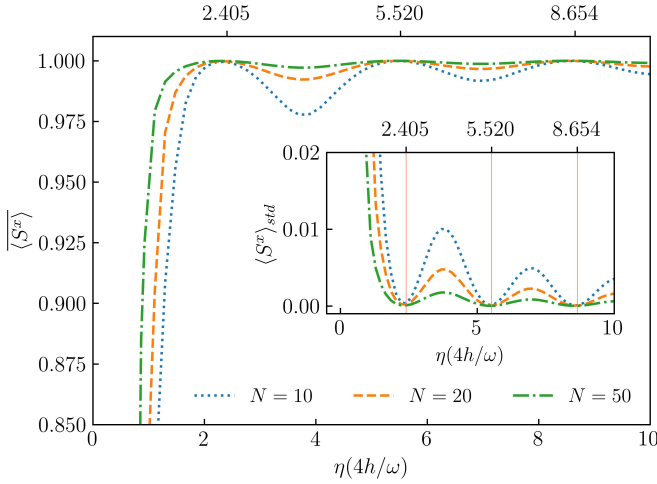


FIG. 4. Temporal average of  $\langle \hat{S}^x \rangle$  (ordinate) for different  $\eta$ 's (abscissa) is plotted for  $\sim 200$  time periods at higher  $\omega$  for different  $N=10,20,50$ .  $\langle \hat{S}^x \rangle$  is unity at roots of  $J_0(\eta)$  (inset panel, red vertical solid line).  $\langle \hat{S}^x \rangle$  is found to fall below unity at points other than roots of  $J_0(\eta)$ .

384  $m$ . The dashed vertical lines correspond to the roots  
 385 of  $J_0(\eta)$ . Comparing with the IPR of the TFIM in fig 1,  
 386 we can see a very similar patterns in the immediate  
 387 neighbourhood of the roots. Evidently, the IPR ap-  
 388 proaches a value of one for sufficiently large values of  
 389 the roots, strongly suggesting full DMBL. Deviations  
 390 occur at the smallest root of  $J_0(\eta)$  (around  $\eta = 2.405$ )  
 391 due to the contributions from higher order terms in  
 392 eq 24. Thus, a higher root is favored for DMBL.

393 The bottom panel of fig 3 contains cross sections  
 394 of the full IPR plot for selected values of  $\eta$  as indi-  
 395 cated in the legend. When the drive amplitude  $h$  is  
 396 adjusted such that  $\eta$  is close to a root of  $J_0(\eta)$ , the Flo-  
 397 quent States are mixed, but not entirely thermal, since  
 398 the IPR does not fall to  $\mathcal{O}(N^{-1})$ , indicating that local-  
 399 ization persists to some extent. However, the further  
 400 we are from the roots, the closer the IPR gets to one  
 401 predicted by thermalization.

402 Figure 4 shows plots of the long-time average (from  
 403  $t = 0 - 200T$ ) of the field amplitude  $\langle \hat{S}^x \rangle$  as a function  
 404 of  $\eta$ . The system is started from the fully polarized  
 405 state  $s_n = N/2$  in the TSS and the dynamics simulated.  
 406 The average is plotted for different values of ampli-  
 407 tude  $h$ , keeping the frequency fixed at a high value of  
 408  $\omega = 90$ . It is clearly very close to unity at roots of  $J_0(\eta)$   
 409 and falls at points away from it, indicating that  $S^x$  is  
 410 approximately conserved at the localization points.

411 Small deviations do occur due to the role of higher  
 412 order terms in the rotated Hamiltonian in eq 23. This  
 413 can be demonstrated quantitatively by comparing the  
 414 IPR obtained from the exact dynamics simulation with  
 415 that obtained from the dynamics of  $\tilde{H}(t)$  in eq 23 after

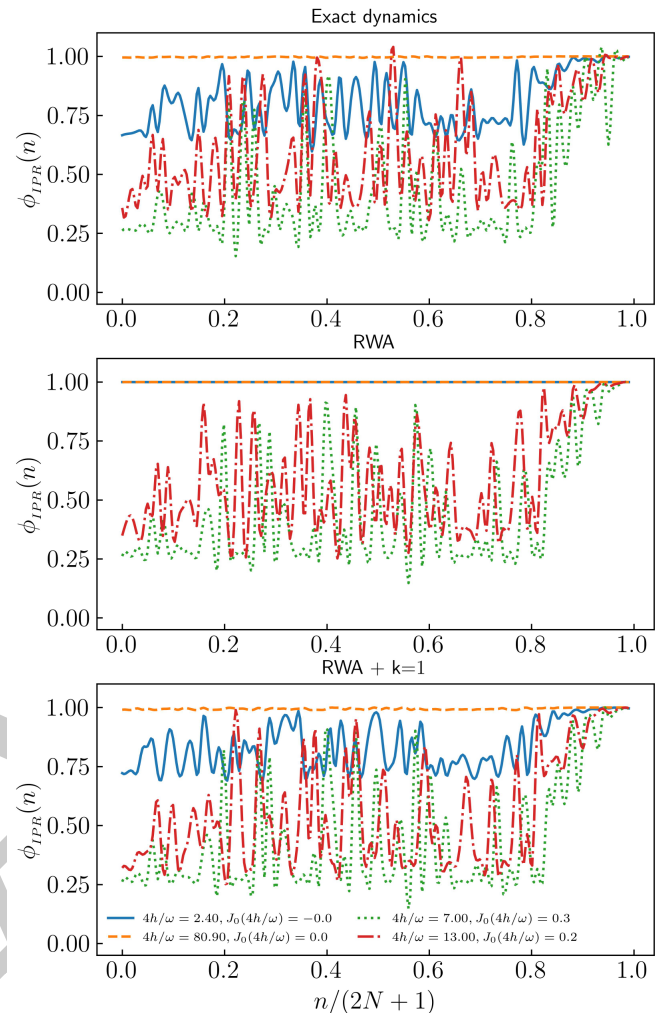


FIG. 5. The comparison between IPR for exact dynam-  
 ics and RWA with corresponding correction orders. IPR is  
 calculated for four different  $\eta$ 's and corresponding  $J_0(\eta)$   
 values for colors, Blue : $\eta = 2.40, J_0(\eta) = 0.0$ , dashed  
 orange: $\eta = 80.9, J_0(\eta) = 0.0$ , Green: $\eta = 7.0, J_0(\eta) = 0.3$ ,  
 Red: $\eta = 13, J_0(\eta) = 0.2$ . At low root of  $J_0(\eta)$  IPR is not unity  
 (Blue curve) where at higher root (orange dashed) it is unity  
 while at points away from roots IPR are less than unity in  
 the exact (top panel) plot. RWA does not matches with the  
 exact plot. At all roots of  $J_0(\eta)$  IPR is unity(middle panel).  
 RWA with additional higher order terms exhibit similar sys-  
 tem pattern(Bottom panel) with exact dynamics.

416 truncating the series at orders  $k \geq 1$ . This compari-  
 417 son can be seen in fig 5. The IPR plots from the ex-  
 418 act dynamics indicate that the first localization point,  
 419 represented by the lowest root of  $J_0(\eta)$ , does not show

complete DMBL. However, DMBL is particularly conspicuous at large roots. The IPRs of the Floquet states obtained from the RWA dynamics exhibit large deviations from unity when away from the localization point as evidenced by the green and red curves in the middle panel of fig 5. However, complete localization is seen in the RWA dynamics at any localization point, in contrast to the exact case in the top panel. Thus, it is necessary to incorporate higher-order corrections into the Rotating Wave Approximation (RWA) at lower localization points. The application of the first-order correction to RWA in the lower panel of fig 5 results in a curve structure that is closer to that from the exact dynamics.

### III. PERSISTENCE OF DMBL IN THE CONTINUUM LIMIT

In the continuum limit, where  $N \rightarrow \infty$ , the disparity between neighboring values of  $s_i$  in equation 20 can be disregarded, and  $s_i$  can be mapped to a continuum  $q \in [-1/2, 1/2]$  [40]. We define the Hamiltonian per particle  $h(t) \equiv \frac{H(t)}{N}$ , and a canonically conjugate co-ordinate  $p \equiv \langle -i/N \frac{\partial}{\partial q} \rangle$ . Then, in this limit, the dynamics can be approximated by that of a classical Hamiltonian [42]

$$h(t) = -2q^2 - [h \cos \omega t + h_0] \sqrt{1 - 4q^2} \cos p, \quad (28)$$

which yields the dynamical system

$$\begin{aligned} \frac{dq}{dt} &= \frac{\partial h}{\partial p} = h(t) \sqrt{1 - 4q^2} \sin p \\ \frac{dp}{dt} &= -\frac{\partial h}{\partial q} = 4q \left[ 1 - \frac{h(t) \cos p}{\sqrt{1 - 4q^2}} \right]. \end{aligned} \quad (29)$$

We have profiled simulations of the ensuing dynamics with the *Poincaré surface of section* (PSOS) of the full dynamics. Here, the  $(q, p)$ -phase space is strobed at  $t = nT$ , and plotted for a large number of initial conditions. The results are shown in the upper panels of fig 6 for a small value of  $\omega = 2.5$  (left panel) and a large value  $\omega = 90.0$  (right panel). In both cases, the value of  $h$  is chosen such that  $\eta$  lies on the first root of  $J_0(\eta)$ . The onset of chaos for small drive frequency indicates thermal behaviour for typical initial conditions, with small islands of regularity for others. This is consistent with similar results for small frequencies reported in [39, 43]. However, at high frequency, the regular islands distinctly dominate over the chaos. The trajectories indicate that the conservation of  $\langle S^x \rangle \approx \sqrt{1 - 4q^2} \cos p$  [40] at high  $\omega$  persists in the thermodynamic limit. That this is a significant nature of the underlying quantum dynamics can be

readily seen in the quantum phase space representation of the Floquet Eigenstates for a large but finite  $N$ . These are shown in the corresponding lower panels of fig 6. Here, we have plotted the Spectral Average of the Husimi Q-functions of the acquired Floquet States in the TSS. Specifically, for a coherent state  $|q, p\rangle$ , the corresponding Spectral-Averaged Husimi distribution [44] is obtained by

$$H(q, p) \equiv \frac{1}{(2N+1)\pi} \sum_n \langle q, p | \phi^n \rangle \langle \phi^n | q, p \rangle \quad (30)$$

The quantum phase space retains signatures of the classical phase space dynamics when  $N = 500$ , indicating the onset of the persistence of  $S^x$  conservation that arises from the resonance condition at high frequencies.

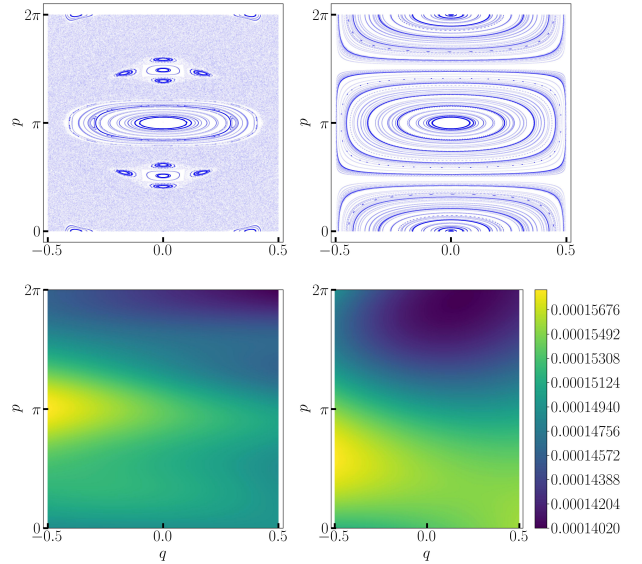


FIG. 6. Phase-space distributions at  $\omega = 2.5$  (left panels) and  $\omega = 90.0$  (right panels) for 100 initial conditions. At small  $\omega$ , the classical PSOS, obtained from simulating the dynamics in eqns 29 (top left panel), shows chaotic behaviour, whereas at the higher  $\omega$ , the onset of regular dynamics can be readily seen (top right panel). The bottom panels plot the corresponding Spectral-Averaged Husimi-Q function, obtained from the Floquet modes  $|\phi^n\rangle$  using eqn 30. The  $\omega = 2.5$ -case (bottom left panel) has a uniform distribution with less contrast in colour. This is consistent with the chaotic behaviour seen in the continuum limit. In the  $\omega = 90$ -case (bottom right panel), the distribution has distinct colour contrasts, which is consistent with the regular dynamics pattern seen in the continuum limit.

#### 478 IV. PHASE CROSSOVER FROM THERMAL TO DMBL

479 The analysis of the periodically driven LMG model  
 480 reveals two distinct scenarios at low and high external  
 481 drive frequencies. In the former case, thermalization  
 482 in accordance with FETH is seen, whereas in the latter  
 483 case, DMBL is induced. As a result, we hypothesize  
 484 that a macroscopic change in phase occurs due to the  
 485 influence of frequency.

486 To demonstrate this, we investigate the IPR of the  
 487 Floquet mode with smallest quasienergy for numerous  
 488 frequencies and system sizes, along with the associ-  
 489 ated drive amplitude  $h$  keeping the system at a local-  
 490 ization point. The results are shown in fig 7. In the  
 491 low-frequency range  $\omega \in [1.0, 9.0]$ , the IPR exhibits val-  
 492 ues well below unity. Moreover, the IPR gradually di-  
 493 minishes with increasing system size, following a sys-  
 494 tem size inverse proportional trend, which confirms  
 495 the participation distribution (as shown in the bottom  
 496 panel). As the limit  $N \rightarrow \infty$ , the inverse participation  
 497 ratio (IPR) tends towards zero, indicating a fully de-  
 498 localized state. The plots reveal a gradual increase in  
 499 the unity of IPR over a certain frequency range, specif-  
 500 ically at  $\omega \approx 5.0$ . In addition, the rise does not cross  
 501 with those for different values of  $N$ , suggesting the  
 502 onset of a phase crossover [27, 45]. As the size of  
 503 the system increases, the crossover region becomes  
 504 smoother, rather than sharper.

505 We can also look at this crossover more clearly in  
 506 the plots of the heating rate of the system, defined  
 507 simply by the expectation value of the Hamiltonian,  
 508  $\langle \hat{H}(t) \rangle$ . We have carried out the numerical eval-  
 509 uation from the simulated dynamics over  $t = 500T$ .  
 510 When the system is adequately described by FETH,  
 511 the temporal fluctuations in the heating rate, defined  
 512 by  $\langle H \rangle_{std}^2 \equiv \overline{\langle \hat{H} \rangle^2} - \overline{\langle \hat{H} \rangle}^2$  (see eqn 3), are minimal in  
 513 the thermodynamic limit, as the spread of states leads  
 514 to a limited standard deviation[46]. Conversely, the  
 515 onset of athermalism is indicated by nonzero fluctua-  
 516 tions in time. If we set the initial state to the fully po-  
 517 larized state in the TSS (given by  $|s_N\rangle$ ), then the onset  
 518 of freezing, together with DMBL, will result in nearly  
 519 infinite hysteresis in the ensuing dynamics, causing  
 520  $|\psi\rangle(t) \approx |s_N\rangle \forall t$ . From eqn 17, we can clearly see that  
 521 this will lead to a linearly rising dependence on  $\omega$  in  
 522  $\langle H \rangle_{std}$  as long as we stick to a localization point given  
 523 by a fixed  $h/\omega$ . All these observations are corroborated  
 524 by the heating rate plots in figure 8.

Review  
from  
here

#### 529 V. OBSERVATIONS AND DISCUSSION

530 The quantum many-body localization in the Ising  
 531 model is observed at high drive frequency and cor-

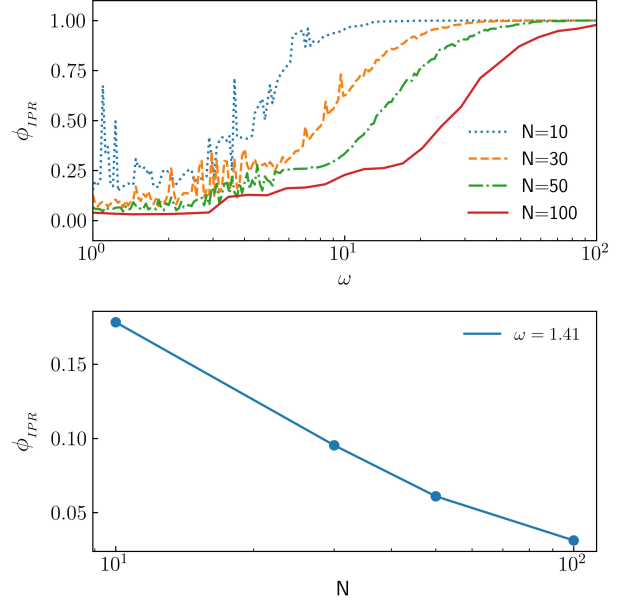


FIG. 7. IPR is plotted (top panel, ordinate) for a range of  $\omega \in [1, 100]$  (top panel, abscissa) for four different  $N = 10, 30, 50, 100$  at root of  $J_0(\eta)$ . At small  $\omega$  upto  $\omega \sim 10$  IPR founds to be very small and rises slowly upto unity (fully localized) at higher frequencies. At bottom panel IPR (ordinate) is plotted for different  $N = 10, 30, 50, 100$  (bottom panel, abscissa) for a random small  $\omega \sim 1$  at root of  $J_0(\eta)$  from the values from top panel. IPR falls as proportional to inverse of  $N$ 's value which is a fully distributed state. The smooth rise in IPR defines a phase cross over (top panel) between a fully distributed thermal phase to a fully localized freezing phase.

532 responding high drive amplitude, where the localiza-  
 533 tion points are determined by setting  $J_0(2h/\omega) = 0$   
 534 for both exact and Rotated wave simulations. The de-  
 535 localization away from the localization points is rela-  
 536 tively weak. The integrability of the Ising model al-  
 537 lows for localization to be observed at low values of  $\omega$ ,  
 538 despite the breakdown of the rotating wave approxi-  
 539 mation. Analytical methods beyond the adiabatic limit  
 540 are intricate. The LMG model exhibits distinct local-  
 541 ization at localization points, which are determined by  
 542 the condition  $J_0(4h/\omega) = 0$ , in both the exact and Ro-  
 543 tated Wave simulations. However, there is some de-  
 544 gree of delocalization observed beyond these points,  
 545 albeit weak. The non-integrability of the LMG model  
 546 and the established onset of chaos in the thermody-  
 547 namic limit at low  $\omega$  lead to a near-complete delocal-  
 548 ization in the Inverse Participation Ratio (IPR) of the  
 549 Floquet states at small  $\omega$ .

550 Consequently, we adiabatically varied  $\omega, h$  in the  
 551 LMG model, under the constraint that  $\eta = 4h/\omega$   
 552 was held at a root of  $J_0(\eta)$ . There, we observed a  
 553 crossover or phase change from nearly fully thermal

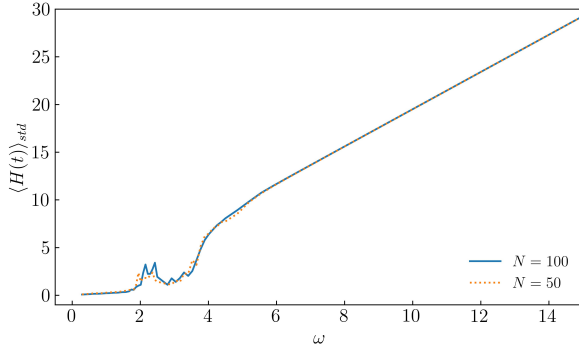


FIG. 8. The standard deviation of the heating rate, denoted by  $\langle H \rangle_{std}$ , calculated over a span of  $t = 500T$  for two system sizes. Here,  $h$  is varied to keep  $\eta = 4h/\omega$  at the first root of  $J_0(\eta)$ . A nonsingular rise has been identified at  $\omega \approx 4.0$ .  $\langle H \rangle_{std}$  exhibits a diminutive magnitude below that value of  $\omega$ , while a linear rise is observed at higher frequencies, consistent with freezing. A vanishingly small standard deviation for  $\omega \ll 4.0$  indicates the presence of a thermal region, whereas a larger finite standard deviation suggests the existence of athermal behaviour. The small peaks observed at  $\omega \in [2, 4]$  are finite-size effects that disappear in the thermodynamic limit.

to completely localised behaviour (see FIG.7). Even if the limitation is relaxed, the macroscopic behaviour changes from thermal to athermal. At low frequencies, IPR is observed to decrease with increasing system size  $N$ , and when  $N$  is big, i.e.,  $\rightarrow \infty$ , IPR appears to evaporate, resulting in a fully thermalized state at  $\eta = 4h/\omega$ . This is in contrast to the Ising model, which lacks such a change in phase. Thus, the incorporation of long-range interactions appears to trigger a change in phase from the thermal phase to the localised phase, a property that will prove useful in the design of MBL engines.

## VI. CONCLUSION AND OUTLOOK

The study delved into the onset of Dynamical Many-Body Localization in the Lipkin-Glick-Meshkov spin model, specifically in regularly driven long-range spins, serving as a paradigmatic illustration. The parametrization of many-body localization is based on the Inverse Participation Ratio of the Floquet eigenstates. The present study conducted a numerical comparison between the inverse participation ratio (IPR) of the LMG model and the transverse field Ising model (TFIM) at both low and high drive frequencies. The present study involved an examination of the phase space dynamics of the LMG model. Specifically, we sought to analyze the emergence of thermal behavior at low frequencies and localization at high frequen-

cies, as well as the appearance of additional approximately conserved quantities in the high-frequency regime for both models.

**Conclusion:** Long-range spins exhibit strong localization in spin-coordinate space for the LMG model when the drive frequency is  $\omega \gg J$ , where  $J$  represents the spin exchange energy. The localization of the LMG model occurs at specific resonances of the drive frequency  $\omega$  and amplitude  $h$ , where  $J_0(4h/\omega) = 0$ . The TFIM case has shown comparable localization (in momentum space) at resonances determined by  $J_0(2h/\omega) = 0$ . However, the mechanism differs in long-range systems as a distinct observable ( $S_x^2$ ) is conserved in the LMG case, where  $S$  represents the total spin. Upon the removal of accidental degeneracy through the application of a DC transverse field in the form of  $\sim S_x$ , the eigenstates can be mapped into a coordinate representation, leading to a robust spatial localization. The periodically driven LMG model exhibits a pronounced mobility edge when the frequency is gradually increased from  $\omega \sim J$  to  $\omega \gg J$  in an adiabatic manner. In the first region where frequency  $\omega$  is small, the quantum system is expected to undergo thermalization at exceedingly high temperatures due to the attainment of dynamical chaos in classical dynamics. However, in the latter high frequency regime, the perpetual postponement occurs due to dynamical localization. The point of transition in mobility between these two regimes exhibits anomalous characteristics when analyzed in the context of thermodynamic principles, indicating a quantum change in phase which detected as *phase – crossover* between them. The absence of thermal behavior in the low-frequency limit of the short-range transverse field Ising model (TFIM) can be attributed to the significant magnitude of the inverse participation ratio (IPR). The induction of Thermal and Localized states in long-range systems can be achieved through Floquet engineering, without the need for disorder.

**Outlook:** A system characterized by high symmetry has been thoroughly examined in a pristine state. Thermalization takes place in all scenarios, alongside integrability-disrupting factors, such as disorder. However, akin to TFIM, the onset of thermalization in LMG can be postponed when the condition  $\omega \gg J$  and  $J_0(4h/\omega) = 0$  is satisfied. In systems possessing a Hamiltonian of the form given by equations 18 and 19, the time-independent Schrödinger equation can be solved analytically for certain potentials. The intermediate spin-spin interaction power law limits have received less attention compared to the infinite and long-range limit. Further research can be conducted on this topic. The LMG spin configuration undergoes a phase cross-over due to the adiabatic increase in drive frequency. This suggests the possibility of a future

636 MBL engine that can operate between the thermal 643 for providing computational resources. AR acknowl-  
 637 and localized regimes, with a thermodynamic cycle. 644 edges support from the University Grants Commis-  
 638 Additionally, there exist prospects for diabatic correc- 645 sion (UGC) of India, via BSR Startup Grant No. F.30-  
 639 tions. 646 425/2018(BSR), as well as from the Science and Engi-  
 640 **Acknowledgement:** One of the authors, MR would 647 neering Research Board (SERB) Core Research Grant  
 641 like to acknowledge The University of Burdwan for 648 No. CRG/2018/004002.  
 642 support via a state-funded fellowship, as well as

- 649 [1] P. Bordia, H. Lüschen, U. Schneider, M. Knap, and 691 [24] M. Bukov, L. D'Alessio, and A. Polkovnikov, ArXiv:  
 650 I. Bloch, *Nature Phys.* **13**, 460. 692 1407.4803v2.  
 651 [2] S. Sahoo, I. Schneider, and S. Eggert, Periodically 693 [25] L. D'Alessio and M. Rigol, *Phys. Rev. X* **4**, 041048  
 652 driven many-body systems: A floquet density matrix 694 (2014).  
 653 renormalization group study (2019), arXiv:1906.00004 695 [26] R. Yousefjani, S. Bose, and A. Bayat, *Phys. Rev. Res.* **5**,  
 654 [cond-mat.str-el]. 696 013094 (2023).  
 655 [3] A. Das, *Phys. Rev. B* **82**, 172402 (2010). 697 [27] P. Sierant, M. Lewenstein, A. Scardicchio, and J. Za-  
 656 [4] G. B. Mbeng, A. Russomanno, and G. E. Santoro, The 698 krzewski, *Phys. Rev. B* **107**, 115132 (2023).  
 657 quantum ising chain for beginners, arXiv:2009.09208. 699 [28] S. Rozhin, Abolfazl 10.1103/PhysRevRe-  
 658 [5] H. S. Yamada and K. S. Ikeda, *Phys. Rev. E* **105**, 700 search.5.013094.  
 659 054201. 701 [29] L. N. Alet Fabien **19**, 10.1016/j.crhy.2018.03.003.  
 660 [6] A. Roy and A. Das, *Phys. Rev. B* **91**, 121106. 702 [30] S. J. Garratt and S. Roy, *Phys. Rev. B* **106**, 054309.  
 661 [7] H. Li, B. Shapiro, and T. Kottos, *Phys. Rev. B* **98**, 703 [31] R. B. Stinchcombe, *J. Phys. C: Solid State Phys.* **6**, 2459.  
 662 121101 (2018). 704 [32] F. E. H. George Arfken, Hans Weber, *Mathematical  
 663 [8] A. Eckardt and E. Anisimovas, *New J. Phys.* **17**, 093039 705 Methods for Physicists*, 7th ed. (Academic Press).  
 664 (2015). 706 [33] S. Mukherjee, A. Spracklen, D. Choudhury, N. Gold-  
 665 [9] L. Zhang, V. Khemani, and D. A. Huse, *Phys. Rev. B* **94**, 707 man, P. Öhberg, E. Andersson, and R. R. Thomson, *New  
 666 224202 (2016). 708 J. Phys.* **17**, 115002.  
 667 [10] V. Khemani, A. Lazarides, R. Moessner, and S. Sondhi, 709 [34] S.-H. Lin, B. Sbierski, F. Dorfner, C. Karrasch, and  
 668 *Phys. Rev. Lett.* **116**, 250401. 710 F. Heidrich-Meisner, *SciPost Physics* **4**, 002.  
 669 [11] N. Yunger Halpern, C. D. White, S. Gopalakrishnan, and 711 [35] N. C. Murphy, R. Wortis, and W. A. Atkinson, *Phys. Rev.*  
 670 G. Refael, *Phys. Rev. B* **99**, 024203. 712 **B** **83**, 184206.  
 671 [12] A. Campa, T. Dauxois, and S. Ruffo, *Physics Reports* 713 [36] E. J. Torres-Herrera, I. Vallejo-Fabila, A. J. Martínez-  
 672 **480**, 57. 714 Mendoza, and L. F. Santos, *Phys. Rev. E* **102**, 062126.  
 673 [13] T. Eisele and R. S. Ellis, *J Stat Phys* **52**, 161. 715 [37] N. Trivedi and D. Heidarian, *Progress of Theoretical  
 674 [14] A. Canning, *Physica A: Statistical Mechanics and its 716 Physics Supplement* **160**, 296.  
 675 Applications **185**, 254. 717 [38] G. Misguich, V. Pasquier, and J.-M. Luck, *Phys. Rev. B*  
 676 [15] D. Vu, K. Huang, X. Li, and S. Das Sarma, *Phys. Rev.* 718 **94**, 155110.  
 677 *Lett.* **128**, 146601 (2022). 719 [39] A. Russomanno, R. Fazio, and G. E. Santoro, *EPL* **110**,  
 678 [16] G. Misguich, V. Pasquier, and J.-M. Luck, *Phys. Rev. B* 720 37005.  
 679 **94**, 155110 (2016). 721 [40] T. Mori, *J. Phys. A: Math. Theor.* **52**, 054001.  
 680 [17] M. Calixto and E. Romera, *J. Stat. Mech.* **2015**, P06029. 722 [41] J. Johansson, P. Nation, and F. Nori, *Computer Physics  
 681 [18] K. Fujii, *Journal of Modern Physics* **8**, 2042. 723 Communications* **184**, 1234.  
 682 [19] D. A. Abanin, E. Altman, I. Bloch, and M. Serbyn, *Rev.* 724 [42] B. Sciolla and G. Biroli, *Phys. Rev. Lett.* **105**, 220401.  
 683 *Mod. Phys.* **91**, 021001 (2019). 725 [43] R. A. Kidd, M. K. Olsen, and J. F. Corney, *Phys. Rev. A*  
 684 [20] M. Srednicki, *Phys. Rev. E* **50**, 888. 726 **100**, 013625 (2019).  
 685 [21] M. Srednicki, *Journal of Physics A: Mathematical and 727 [44] A. Bäcker, S. Fürstberger, and R. Schubert, *Phys. Rev.*  
 686 General* **32**, 1163 (1999). 728 **E** **70**, 036204 (2004).  
 687 [22] M. Holthaus, *J. Phys. B: At. Mol. Opt. Phys.* **49**, 013001 729 [45] S. Sachdev, *Quantum Phase Transitions*, 2nd ed. (Cam-  
 688 (2016). 730 bridge University Press, Cambridge, 2011).  
 689 [23] M. Vogl, M. Rodriguez-Vega, and G. A. Fiete, *Phys. Rev.* 731 [46] P. Reimann, *J. Stat. Mech.* **2021**, 103106.  
 690 *B* **101**, 024303 (2020).*